*Sensors and Materials*, Vol. 36, No. 7 (2024) 2765–2781
MYU Tokyo



S & M 3700

# Technology for Sensing and Reducing Noise in Acoustic Emission Signals for Online Detection of Wear Condition of Transmission Gears in a Nuclear Power Plant

Long Wu,[1] Kun-Chieh Wang,[1*] Hao Gao,[1]
Lei Qiang,[1,2] and Chi-Hsin Yang[1]

[1]School of Mechanical and Electric Engineering, Sanming University, Sanming 365004, Fujian Province, China
[2]College of Mechanical and Electrical Engineering, Fujian Agriculture and Forestry University, Fuzhou 350002, Fujian Province, China

(Received January 3, 2024; accepted July 9, 2024)

***Keywords:*** nuclear power plant, wear condition of gears, noise reduction, acoustic emission

Once a nuclear power plant is started, its power transmission devices need to be kept running for a long time without stopping. Currently, the wear condition of gears in the transmission gear box of a nuclear power plant cannot be monitored in real time. An unexpected stoppage due to the damage of power transmission gears would cause significant losses. To solve this problem, we propose a novel technology for sensing and reducing the noise in acoustic emission (AE) signals, which may be used to effectively detect, analyze, and monitor the surface friction condition of transmission gears in a nuclear power plant in real time. In this study, we first analyze the crucial factors that affect the signal energy of AE from the contact surface of teeth via the Hertz contact theory. Second, we propose a novel noise reduction method to deal with the detected AE signals. Third, we establish a mathematical model that correlates the lubricant viscosity, gear load, and the running speed of gears with the energy of AE signals. Fourth, we design a novel AE signal acquisition-analysis system. Finally, we perform verification tests via this system. The results of these tests are satisfactory. Using the proposed sensing and noise reduction methodology, we effectively analyzed the surface wear of transmission gears in a nuclear power plant in real time. Appropriate safety measures can be taken in time on the basis of our monitoring results.

## 1. Introduction

Once a nuclear power plant is started up, its internal power transmission unit needs to run for a long time without interruption. However, the wear and tear of the internal gears of the most critical gearbox equipment responsible for power transmission cannot be monitored in real time during operation. When this power transmission gear is damaged, it can lead to an unexpected shutdown, resulting in a nuclear radiation leakage accident, causing human injuries and

*Corresponding author: e-mail: m18316252102@126.com
https://doi.org/10.18494/SAM4878

ISSN 0914-4935 

economic losses. To address this issue, many scholars have proposed various methods to detect and monitor the wear condition of gears, with acoustic emission detection technology being the most popular method.

The acoustic emission technology (AET) scheme was first studied by Kaiser[1] in 1950, who classified the AET scheme into two types: continuous and burst. In 1964, American researchers applied the AET scheme to detect the mass of a rocket engine housing. Because the AET scheme has strong anti-interference ability, it developed rapidly and was then successfully applied to the industrial field.[1] In the wear detection of gears, Guild *et al.*[2] determined the applicable frequency of acoustic emission (AE) signals to be within the range of 100 kHz–1 MHz, laying a foundation for the application of this technology in engineering practice. On the basis of the Hertz contact theory, Ram and Anand[3] studied the relationship between AE signals and tooth profile slip rates, established the relationship model between the tooth profile quality and the tooth profile defect, and applied the AET scheme to gear-fault diagnosis problems. Novoa and Vicuña[4] studied the effects of rotational speed, load, and oil viscosity on oil film thickness and pressure distributions, analyzed the AE signals of a gear box using the AET scheme, and found that the results were close to those obtained using the elastic hydrodynamic lubrication theory and the asperity contact hypothesis. Li *et al.*[5] applied the wavelet transform method to the research on the positioning and detection of gear faults of a split torque gear box. Gu *et al.*[6] applied the discrete wavelet transform scheme to the noise reduction processing of AE signals and carried out the envelope analysis of AE signals for gears, and finally completed the early fault diagnosis of running gears. Prieto and Millán[7] proposed a new fault indicator and a feature estimation method that can detect gear degradation under different working conditions. Mba conducted a comprehensive study on the AET scheme used in the condition monitoring of bearings, pumps, gears, and other rotating machinery, publishing findings on the relationship between AE signals and motor rotors.[8,9]

Moreover, the AET scheme can be applied to many other fields, such as pattern recognition, machine learning, vibration monitoring, and grinding condition detection. Leaman *et al.*[10] proposed a pattern classification method based on the artificial neural network (ANN) for the application of the AET scheme to the recognition of the different working conditions of gears. Their results showed that the ANN-based AET scheme has excellent application potentials. Vicuña[11] used the AET scheme to study the correlation among the lubricating oil temperature, rotational speed, load, and AE signal during the gear meshing operation, and applied the test results to the condition monitoring of the planetary gear box of a bucket-wheel excavator. Tan *et al.*[12] conducted experimental research on the natural pitting of gear surfaces, continuously monitored AE signals, vibration signals, and the spectral information of oil samples for a long time, and compared the measured results with those obtained from the natural life degradation of gears. They found that the AET scheme is more accurate than the vibration monitoring and spectral analysis schemes in the fault detection of the surface pitting of gears. Raghav and Sharma[13] studied the application of the AET scheme in fault diagnosis for different types of transmission device. They discussed the effects of AE signal parameters and the processing technology on the fault diagnosis of transmission devices, studied the feature extraction technology of AE signals, established a suitable model of AE signals, and investigated the

effects of the fault location. Li *et al.*[14] studied the mathematical relationship between the amplitude of AE signals and grinding parameters during machining for a grinding machine.

In summary, although many studies were conducted on the AET scheme applied to different fields, there were few reports on the AET scheme applied to the real-time monitoring of the surface wear of gears in a nuclear power plant. Therefore, this study aims to address this issue. First, in Sect. 2, we discuss the basics of sensing and detection technology for AE signals. Then, in Sect. 3, we describe the methodology of noise reduction of AE signals. Additionally, in Sect. 4, an AE signal acquisition-analysis system is set up using the proposed AET scheme to effectively detect and monitor the surface wear of transmission gears in a nuclear power plant. Real-time experiments are conducted for verification.

## 2. Foundation of Sensing and Detection Technology of AE Signals

### 2.1 Principle

AE refers to the phenomenon of deformation or fracture of parts or materials under the action of internal or external forces, resulting in stress concentration in a local area. When the internal energy of an object is released rapidly, some transient elastic waves are generated, which is called the stress wave emission.[15] The AE phenomenon is commonly seen in practice, such as the sound of wood fracture, gear meshing, and bearing friction. On the basis of some physical principles, the technology that uses hi-tech equipment to collect, process, and analyze the AE signals is called the AET scheme.[16]

The procedure of the AET scheme applied to detect gear-surface conditions is shown in Fig. 1. When the gear material is subjected to external forces, the generated instantaneous elastic waves propagate from inside to the surface of the gear. These elastic waves stimulate the AE

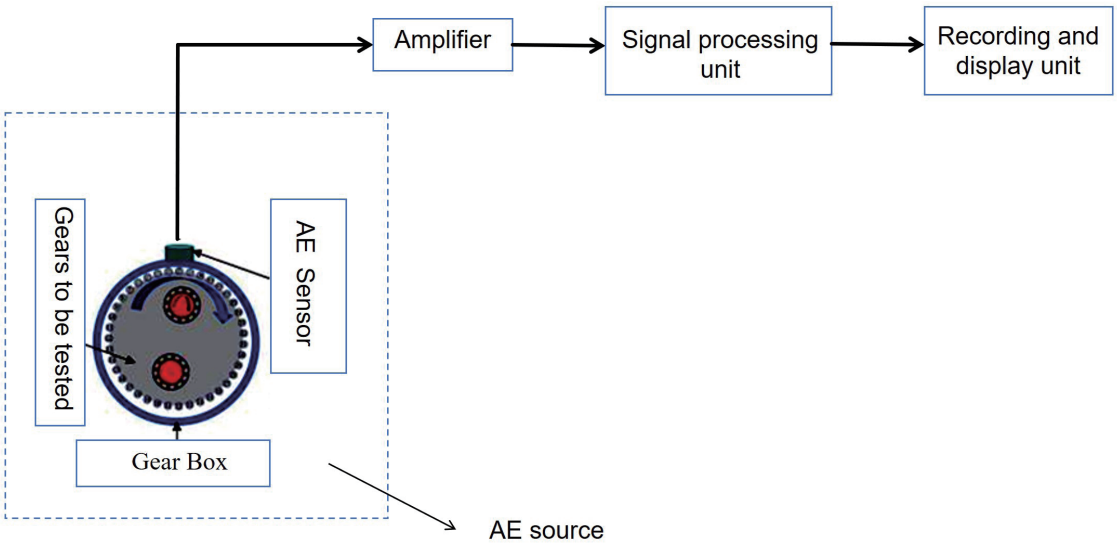


Fig. 1. (Color online) Schematic diagram of AET scheme applied to gear-condition detection.

sensor and induce mechanical vibrations. A vibration signal is thus formed in the AE sensor and then sent to an amplifier, a data processor, and a final recording and displaying unit.

The AE signals can be divided into burst and continuous types according to the change in signal amplitude.[17,18] In general, there are two major data processing methods for AE signals. One is the method of characteristic parameter analysis and the other is the method of waveform analysis.[19] Both methods are adopted in this study. Here, we focus on using the AET scheme to detect and analyze the signal emitted from the wearing surfaces of meshing gears in a planetary gear box and then establish the appropriate relationship between the AE signal and the wear of gear surfaces.

### 2.2 Model

As an important power transmission component in rotating machinery, the mechanical state of running gears can be regarded as a complex nonlinear vibration motion. The main source of AE signals in the gear meshing operation originates from the interaction between two contacting micro-convex bodies appearing on the gear surfaces.[20–22] During the meshing running of gears, the occurrence of elastic deformation, fracture, and adhesion of the contacting micro-convex bodies will result in the formation of high-frequency elastic stress waves (AE signals). In the 1940s, Bowden and Tabor put forward the theory of adhesive friction, which mentioned the stress generated by the action of micro-convex bodies between the contact surfaces of a gear pair.[23,24] Subsequently, Wang *et al.*[25] noted that the surface machining quality of gear parts is closely related to the micro-convex bodies in contact. On the basis of the Greenwood–Williamson contact model and the Hertzian contact theory, Fan *et al.*[26] simulated the wear conditions of metal pieces with rough surfaces in contact and established a relationship among the load, the relative sliding velocity, the surface roughness, and the energy of the AE signal.

According to Fan *et al.*,[26] the elastic energy per unit time generated by friction among micro-convex bodies on the contact surface can be expressed as

$$\bar{U}_{AE} = 0.4 k_e k_m N w v \frac{F_1(h)}{R^{1/2}\, F_{1/2}(h)}, \tag{1}$$

where $k_e$ is the ratio of the transformed $AE$ signal energy to the elastic energy generated by friction on contact surfaces, $k_m$ is the gain of $AE$ signals, $N$ is the number of micro-convex bodies in contact, $w$ is the load applied, $v$ is the relative sliding speed between two surfaces in contact, and $h$ is the thickness of the oil film. The total elastic energy collected by the $AE$ sensor is

$$U_{AE} = \int_0^{\infty} \bar{U}_{AE}\, dt\,. \tag{2}$$

## 3. Methodology of Noise Reduction of AE Signals

To exactly detect the wear conditions of gear-tooth surfaces from the measured AE signals, it is necessary to reduce the signal noise. Here, we propose a novel noise reduction methodology (NRM), which mainly includes the singular value decomposition (SVD) method based on the energy spectrum of the entropy difference (ESED) scheme to reduce the noise of the AE signal data. Comparisons and verification are also made to examine the effectiveness of our proposed methodology.

### 3.1 SVD method

For a group of measured one-dimensional signals $X = [x(1), x(2), x(3), ..., x(N)]$, we may construct a Hankel matrix $H$ according to the phase-space reconstruction principle as[27]

$$H = \begin{bmatrix} \mathrm{x}(1) & x(2) & \cdots & x(n) \\ x(2) & x(3) & \cdots & x(n+1) \\ \vdots & \vdots & \ddots & \vdots \\ x(m) & x(m+1) & \cdots & x(N) \end{bmatrix}. \tag{3}$$

In Eq. (3), $1 < n < N$, $m \geq 2$, $n \geq 2$, and $N = m + n - 1$. According to the SVD theory,[28] there exist the orthogonal matrices $U = (u_1, u_2, \cdots, u_m) \in R^{m \times m}$ and $V = (v_1, v_2, \cdots, v_n) \in R^{n \times n}$, so that the matrix $H$ can be decomposed into

$$H = USV^T, \tag{4}$$

$$S = \mathrm{diag}\,(\sigma_1, \sigma_2, \cdots, \sigma_q, 0), \tag{5}$$

where $U$ is a left singular vector, $V$ is a right singular vector, $S$ is a diagonal matrix ($S \in R^{m \times n}$), and $\sigma_1 \geq \sigma_2 \geq \cdots \geq \sigma_q \geq 0$, $\sigma_i$ ($i = 1, 2, \cdots, q$) is the singular value of matrix $H$, $q = \min(m,n)$. Equation (4) is usually expressed in vector form as

$$H = \sum_{i=1}^{q} H_i = \sum_{i=1}^{q} \sigma_i u_i v_i^T. \tag{6}$$

Xiao *et al.*[29] showed that, for a signal $X$ that contains $I$ frequencies, the total number of $2I$ nonzero singular values can be generated after decomposition by maximizing the number of rows and columns in the Hankel matrix. Accordingly, Eq. (6) can be reconstructed as

$$H_{m \times n} = C_1 + C_2 + \cdots + C_I + \cdots = \sigma_1 u_1 v_1^T + \sigma_2 u_2 v_2^T + \cdots + \sigma_{2I} u_{2I} v_{2I}^T + \sum_{h=2I+1}^{q} \sigma_h u_h v_h^T. \tag{7}$$

Hence, the matrix $H$ is further transformed into two component matrices, as

$$H_{m\times n} = D_{m\times n} + W_{m\times n} = U_{m\times n} S_{m\times n} V_{n\times n}^{T}, \tag{8}$$

where $D$ represents the space of useful signals and $W$ represents the space of noise signals.

### 3.2 ESED scheme for determination of reconstruction order

There are many popular methods[30–33] that can be used to determine the reconstruction order of SVD, such as the mean-value, median-value, asymptotic singular-value, and ESED method. Among these methods, we adopted the ESED method proposed by Sikdar *et al.*[30] in 1948, who used the information entropy to describe the uncertainty of message sources. The higher the certainty of a signal, the lower the information entropy; conversely, the less deterministic (i.e., more random) a signal, the greater its information entropy. Through the information-entropy concept, the signal can be described quantitatively. Normally, the distribution of information-entropy energy has a clear peak at the boundary between signal and noise. The energy of information entropy is expressed as

$$C_i = \sigma_{2i-1} u_{2i-1} v_{2i-1}^{T} + \sigma_{2i} u_{2i} v_{2i}^{T},\ (i = 1, 2, \cdots, I), \tag{9}$$

where $C_i$ is the $i$th frequency component, $\sigma_i$ is the $i$th singular value, $u_i$ is the $i$th left singular vector, and $v_i$ is the $i$th right singular vector. Moreover,

$$E_i = \int \left| C_i \right|^2 dt, \tag{10}$$

$$E = \sum_{i=1}^{I} E_i, \tag{11}$$

$$H_{en} = -\sum_{i=1}^{I} p_i \log(p_i), \tag{12}$$

where $E_i$ is the $i$th energy component, $E$ is the total energy of $E_i$, $H_{en}$ is the information entropy, and $p_i$ is the ratio of component energy to total energy.

$$M(i) = \frac{H_{en}(i) - H_{en}(i+1)}{\sum_{i=1}^{I} H_{en}(i)} \tag{13}$$

The reconstruction point is defined as the point where the maximum peak of $M(i)$ is reached.

### 3.3 Manipulation procedure of NRM

The manipulation procedure of NRM is schematically shown in Fig. 2. First, we establish a Hankel matrix on the basis of the measured noise signal data. Second, we decompose the Hankel matrix via Eqs. (4)–(8) to obtain *U*, *S*, and *V* matrices. Third, the component matrix *C* is formed by taking every two singular values as a set of reconstructed signals. Fourth, we calculate $M(i)$ in Eq. (13). Fifth, we reconstruct the Hankel matrix by the well-known average method.[34]

### 3.4 Verification

To verify our proposed NRM, we adopted the open data of failure bearings published by Du *et al.*[35] In the simulation test, we set the carrier frequency of the bearing as 300 Hz, the average time interval of adjacent shocks in the simulation signal as $\Delta T_i = T_i - T_{i+1} = 1/15$ ($f_i$ = 15 Hz), the sampling frequency as 2000 Hz, and the number of samplings as 1000. The signal model is defined as

$$x(t) = x_0(t) + n(t) \quad t \in (0, 0.5)\,, \tag{14}$$

and

$$x_0(t) = 10e^{-\alpha t} \sin 600\pi t\,. \tag{15}$$

In Eqs. (14) and (15), $x_0(t)$ is the net signal without noise with an amplitude of 10 dB, $\alpha$ is the attenuation coefficient with a value of 80, $n(t)$ is the Gaussian white noise with a signal-to-noise ratio of −5 dB, and $x(t)$ is the simulated signal with noise. The obtained time-domain waveforms of the net signal without and with noise are shown in Figs. 3(a) and 3(b), respectively.

As shown in Fig. 3(b), the characteristics of the net signal $x_0(t)$ are completely submerged by the noise $n(t)$ and thus cannot be recognized. To solve this problem, we adopted the frequency-domain analysis method. Using Eqs. (14) and (15), we obtained the frequency-domain signal with noise, as shown in Fig. 4. It is seen that the characteristics of the signal $x(f)$ can be recognized now but with some defects. Near the pass band of frequency, i.e., low-frequency

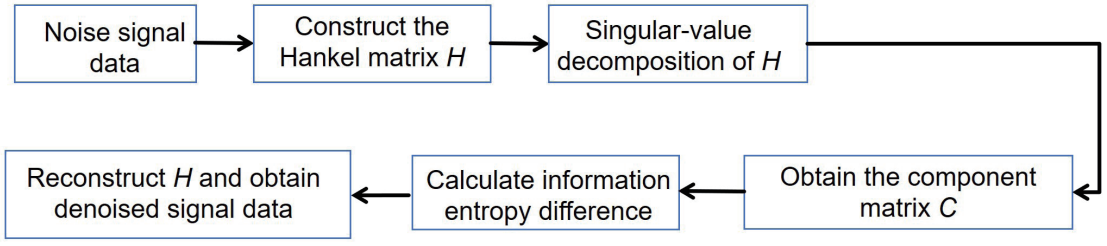


Fig. 2. (Color online) Manipulation procedure of NRM.

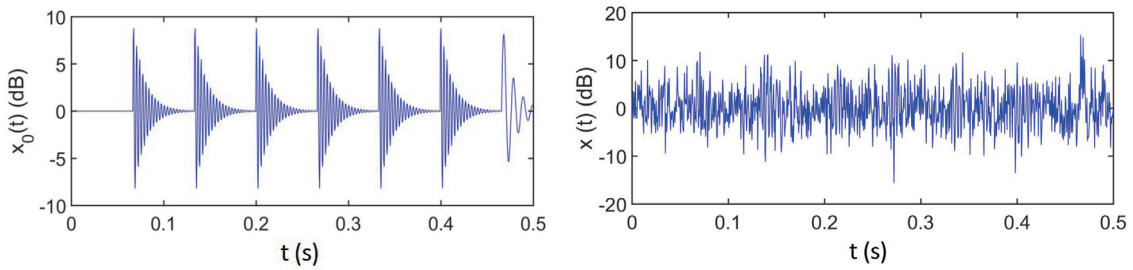


(a) (b)

Fig. 3. (Color online) Time-domain waveforms of net signal: (a) without and (b) with noise.

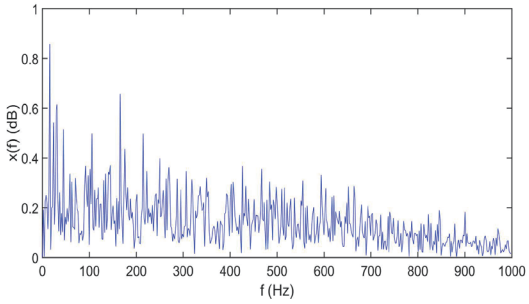


Fig. 4. (Color online) Envelope amplitude spectrum of simulated signals with noise.

region, the characteristics of the signal $x(f)$ are vague because of the interference by noise. Therefore, we need to introduce the ESED method to further reduce this noise.

Through calculations via Eqs. (3)–(13), we first obtained the variation of $M(i)$ with the reconstruction order for the signal with noise, as shown in Fig. 5. Apparently, it is appropriate to choose the reconstruction order as $RO = 5$ in calculations, where the maximum peak of $M(i)$ (0.03608) is reached. Since a single component value corresponds to two singular values, the first ten singular values were taken to reconstruct the original signal with noise. The obtained time-domain waveform of the reconstructed signal with noise is shown in Fig. 6.

Figure 6 shows that the signal reconstruction result is satisfactory, in which the impact characteristics of the signal with noise clearly appear. Next, we further verified the proposed NRM by the correlation method. The correlation coefficients between the reconstructed signals with the reconstruction orders of 2, 5, and 7 and the simulated signal without noise were calculated using the following equation:

$$\rho_{xy} = \frac{Cov(X,Y)}{\sqrt{Var[x]Var[y]}} = \frac{\sum_{n=0}^{+\infty} X(n)Y(n)}{\sqrt{\sum_{n=0}^{+\infty} X^2(n)Y^2(n)}}. \tag{16}$$

The obtained results are shown in Table 1. The closer the correlation coefficient is to 1, the less noise the reconstructed signal contains.

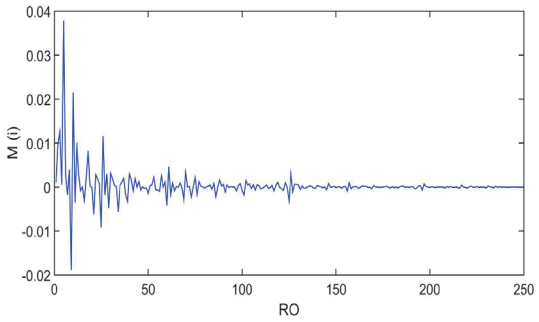


Fig. 5. (Color online) Variation of $M(i)$ with $RO$ for signal with noise obtained using ESED scheme.

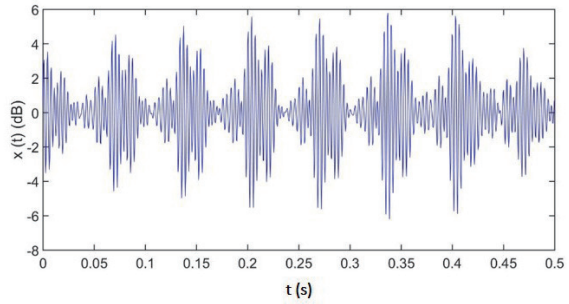


Fig. 6. (Color online) Time-domain waveform of reconstructed signal obtained using ESED scheme.

Table 1
Correlation coefficients for signals with different reconstruction orders.

| Reconstruction order ($RO$) | 2 | 5 | 7 |
|---|---|---|---|
| Correlation coefficient | 0.596 | 0.751 | 0.721 |

Table 1 shows that the highest correlation coefficient (0.751) appears at $RO = 5$ where the maximum peak of ESED is reached, which means that the best noise reduction effect occurs when we adopt $RO = 5$ in signal reconstruction.

Next, to further verify our proposed NRM method, we used the singular-value asymptote (SVA) and singular-value energy difference spectrum (SVEDS) methods to calculate the reconstruction order, and the results obtained are shown in Figs. 7 and 8, respectively.

Figure 7 shows that the reconstruction order obtained by the SVA method is about $RO = 90$ where the asymptote begins to bend. Figure 8 shows that $RO = 4$ is obtained by the SVEDS method. By using these two methods, we obtain the relations of amplitude versus time and envelope amplitude versus frequency, as shown in Figs. 9(a) and 9(b), respectively.

Figure 9 shows that the reconstructed signal still has a lot of noise. In other words, the SVA method exhibits a poor noise reduction effect. On the other hand, Fig. 10 shows that the SVEDS method can extract the failure characteristics of signals, but distorts them. Moreover, we compared the two abovementioned methods, together with the ESED scheme, by calculating the correlation coefficients between the reconstructed signals and the original signal, as shown in Table 2.

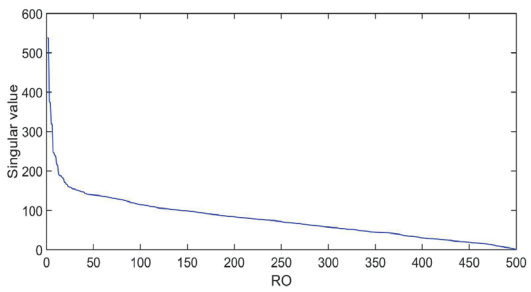


Fig. 7. (Color online) Reconstruction order calculated by SVA method.

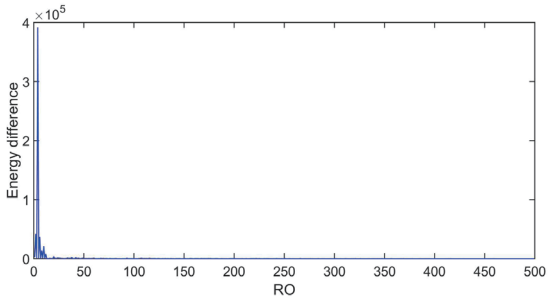


Fig. 8. (Color online) Reconstruction order calculated by SVEDS method.

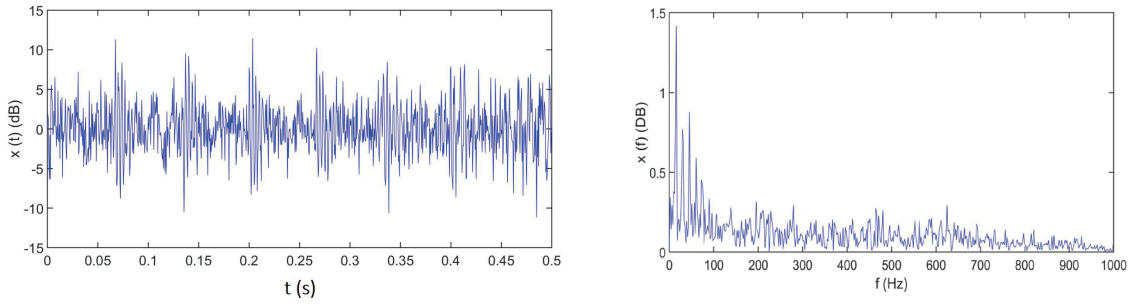


(a) (b)

Fig. 9. (Color online) Reconstructed signals in time and frequency domains obtained by SVA method: (a) time and (b) frequency domains.

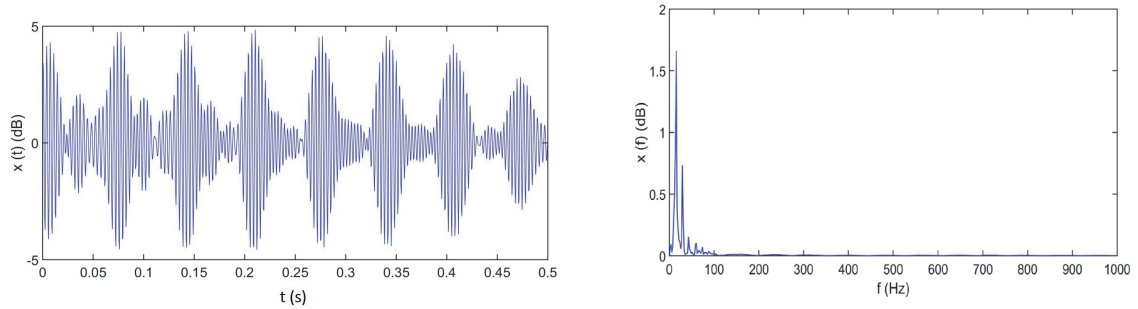


(a) (b)

Fig. 10. (Color online) Reconstructed signals in time and frequency domains obtained by SVEDS method: (a) time and (b) frequency domains.

Table 2
Correlation coefficients obtained by different methods.

| Noise reduction method | SVA | SVEDS | ESED |
|---|---|---|---|
| Correlation coefficient | 0.6 | 0.71 | 0.75 |

By comparing the obtained correlation coefficients in Table 2, it can be seen that the ESED scheme exhibits the highest correlation coefficient (0.75), which is better than those obtained by the SVD (0.6) and SVEDS (0.71) methods. On the basis of the above finding, we concluded that the noise interference can be effectively removed by using the ESED scheme.

## 4. Real-time Experiments

### 4.1 Experimental setup and sensor arrangement

To effectively analyze the surface wear of transmission gears in a nuclear power plant in real time, we specifically carried out some experiments on the sensing and noise reduction of AE signals during gear running in real time. First, we set up an AE signal acquisition-analysis system, which mainly includes a wide-band AE sensor (sensitivity: 70 ± 3 dB), a preamplifier (40 dB bandwidth, 10 kHz–2 MHz), and a set of AE signal acquisition software, as shown in Fig. 11. The experimental parameters include the effects of the lubricant viscosity ($\mu$), gear load ($L$), and motor speed ($V$). We set three types of lubricant: (1) L-TSA32 turbine oil with $\mu$ = 32.5 mm$^2$/s, (2) L-TSA46 turbine oil with $\mu$ = 45.2 mm$^2$/s, and (3) L-TSA68 turbine oil with $\mu$ = 68.9 mm$^2$/s, three types of applied load: (1) 25% $L_{max}$, (2) 50% $L_{max}$, and (3) $L_{max}$, where $L_{max}$ means the maximum rating load, and three types of motor speed: (1) 15, (2) 25, and (3) 50 Hz. Other related experimental conditions were set as follows. The transmission ratio of gears was set to 5.5 and that of the right-angle reducer system was set to 11.17. At high speed, the voltage and frequency were set to 380 V and 50 Hz, respectively. At medium speed, the voltage and frequency were set to 190 V and 25 Hz, respectively. At low speed, the voltage and frequency were set to 114 V and 15 Hz, respectively. Three lubricating oils of the same type with different


(a) (b)

Fig. 11. (Color online) AE signal acquisition-analysis system: (a) major system and (b) AE sensor.

kinematic viscosities at 40 °C were used in the tests, as stated earlier. The sampling frequency was 1 MHz, the preamplifier gain was 40 dB, and the sampling time was 1 s. When ready, we set different experimental parameters as indicated above. Then, we started the equipment and recorded the detected data in groups when the gears ran stably.

### 4.2 Sensor-measurement results and discussion

**Case 1: Effect of motor speed**

We used the L-TSA68 turbine oil as the gear lubricant, the motor speeds were set to 15, 25, and 50 Hz, and there was no load applied. The signals measured by the AE sensors at different speeds in the form of voltage ($E$) versus time ($t$) are shown in Fig. 12. It is seen that the overall maximum absolute voltage of the AE signal gradually increases with motor speed.

On the basis of the above data, we used the proposed ESED scheme with a total of 8192 samples to reduce the noise of the measured AE signals. The resultant time-domain waveform of AE signals after noise reduction is shown in Fig 13. It is seen that, under the no-load condition, the overall voltage of the AE signals after noise reduction increases with motor speed. When the motor speed is as low as 15 Hz (about 218 rpm), the maximum absolute voltage of the reconstructed signal varies within the range of 0.1–0.2 V. When the motor speed increases to 50 Hz (725 rpm), the maximum absolute voltage of the reconstructed signal exceeds 0.2 V.

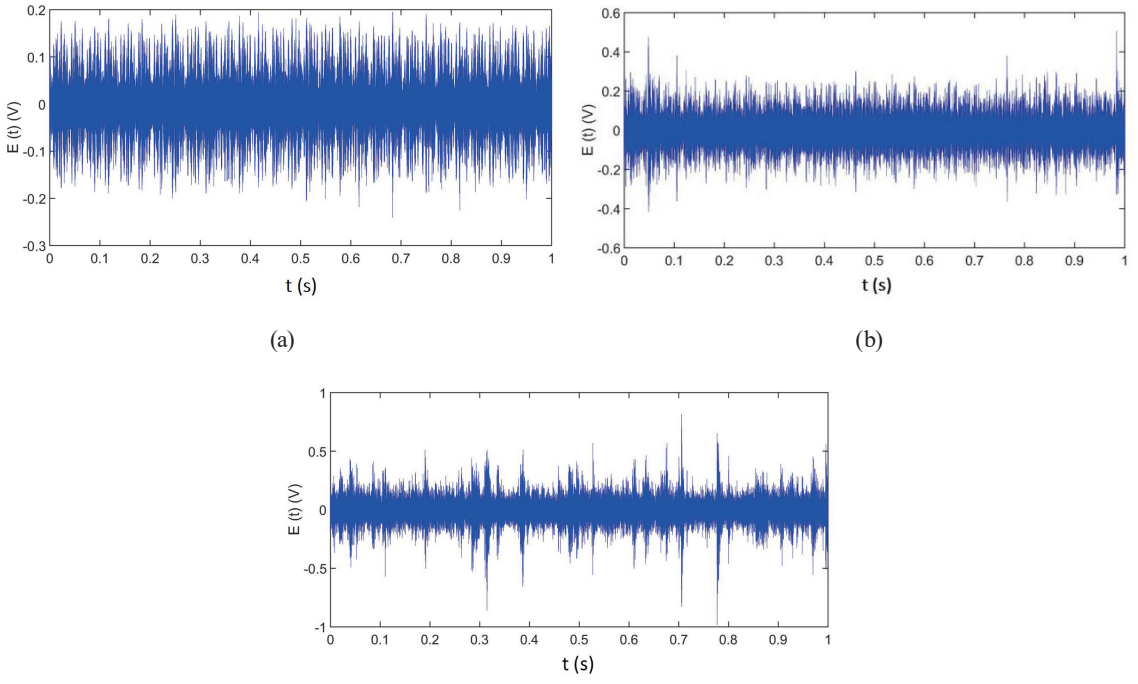


Fig. 12. (Color online) Time-domain waveforms of the measured signal of L-TSA68 turbine oil at different speeds: (a) 15, (b) 25, and (c) 50 Hz.

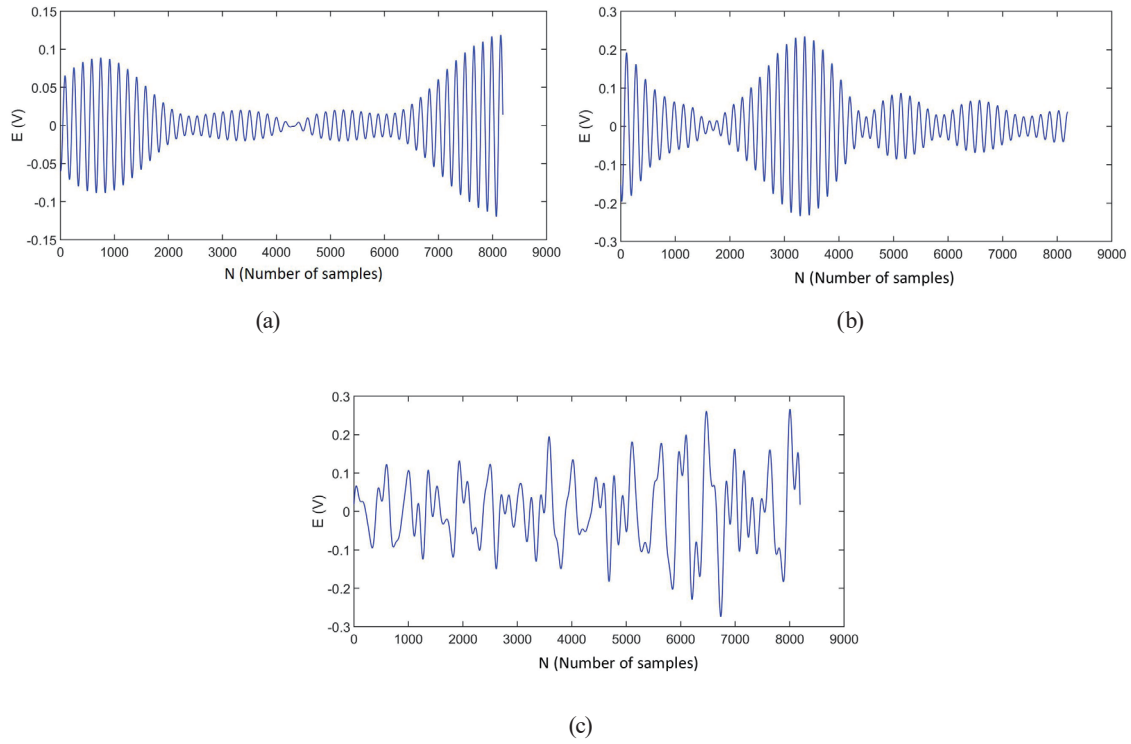


Fig. 13. (Color online) Time-domain waveforms of the reconstructed AE signal of L-TSA68 turbine oil with noise reduction at different speeds: (a) 15, (b) 25, and (c) 50 Hz.

**Case 2: Effect of load**

We used the L-TSA68 turbine oil as the gear lubricant, the motor speed was set to 50 Hz (725 rpm), and the applied load was set to 25% $L_{max}$, 50% $L_{max}$, and $L_{max}$. The signals measured by the AE sensors at different loads in the form of electrical voltage versus time are shown in Fig. 14. It is seen that the maximum absolute electrical voltage of the AE signal gradually increases with applied load. When the applied load is as low as 25% $L_{max}$, the maximum absolute electrical voltage of the reconstructed signal is smaller than 1 V. When the applied load increases to $L_{max}$, the maximum electrical voltage of the reconstructed signal exceeds 2 V.

On the basis of the data shown in Fig. 14, we used the proposed ESED scheme with 8192 samples to reduce the noise of the measured AE signals. The resultant time-domain waveform of the AE signals after noise reduction is shown in Fig 15. It is seen that the amplitude of AE signals with noise reduction increases as the motor speed increases.

**Case 3: Effect of lubricant viscosity**

The motor speed was set to 50 Hz (725 rpm) and the applied load was $L_{max}$. We used three different gear lubricants: L-TSA32, L-TSA46, and L-TSA68 turbine oils. The signals measured by the AE sensors for different lubricants in the form of electrical voltage versus time are shown in Fig. 16. Figure 16 shows that because the viscosity of the adopted lubricant (such as the L-TSA32 turbine oil) is low, the maximum absolute electrical voltage of the AE signal is close to

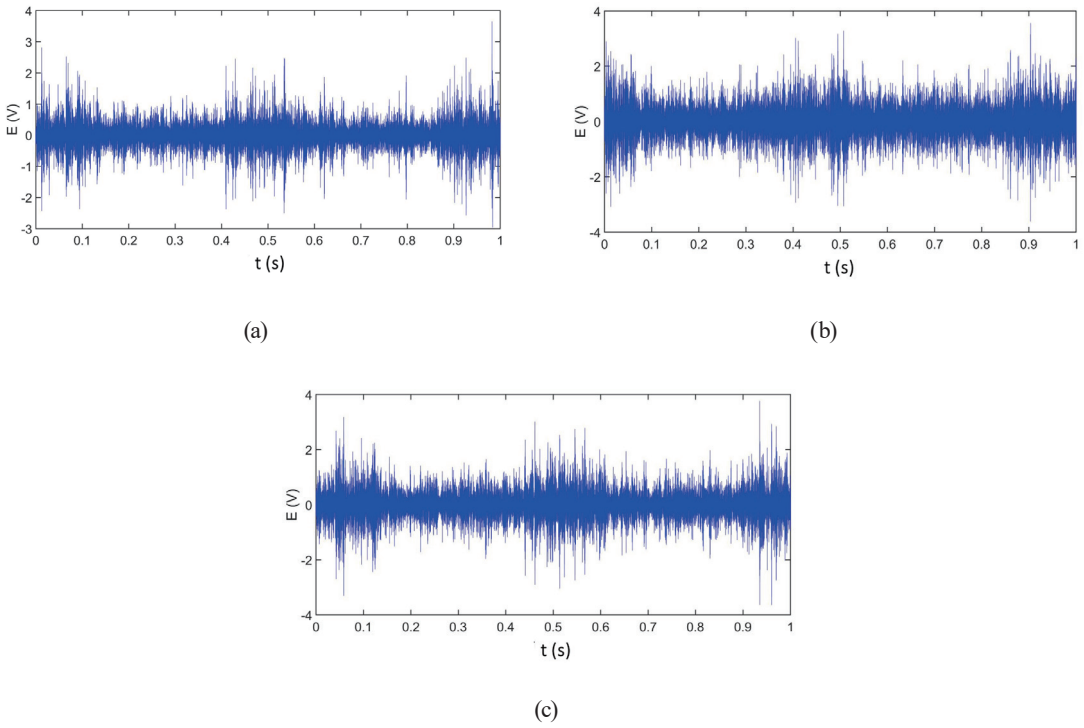


Fig. 14. (Color online) Time-domain waveforms of the measured AE signal of L-TSA68 turbine oil for different loads: (a) 25% $L_{max}$, (b) 50% $L_{max}$, and (c) $L_{max}$.

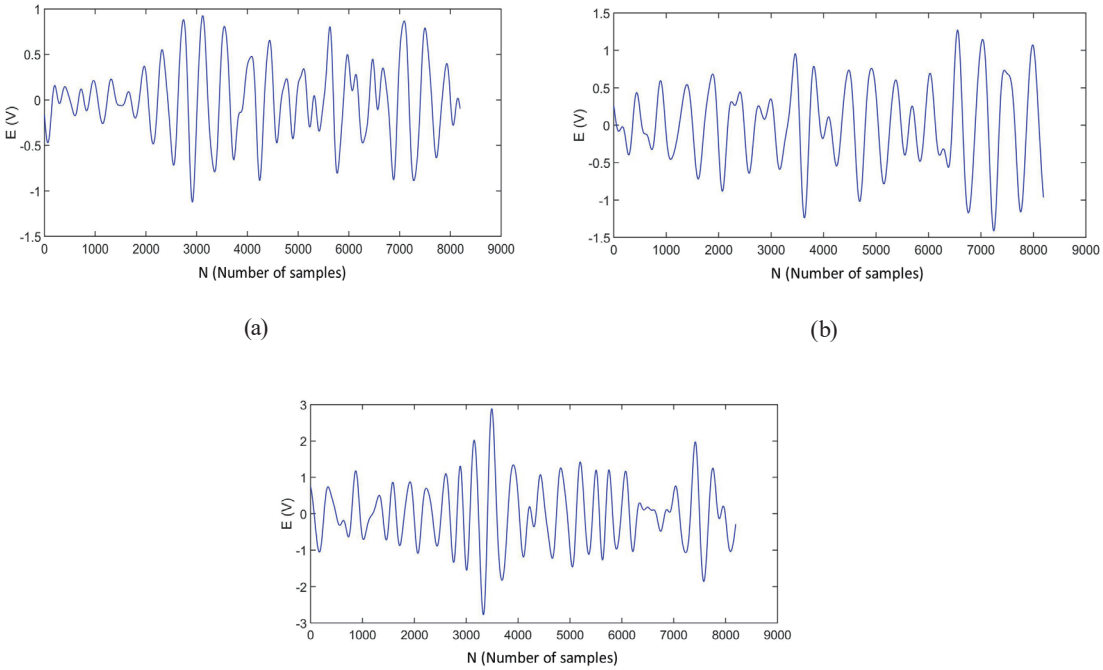


Fig. 15. (Color online) Time-domain waveforms of the reconstructed signal of L-TSA68 turbine oil with noise reduction for different loads: (a) 25% $L_{max}$, (b) 50% $L_{max}$, and (c) $L_{max}$.

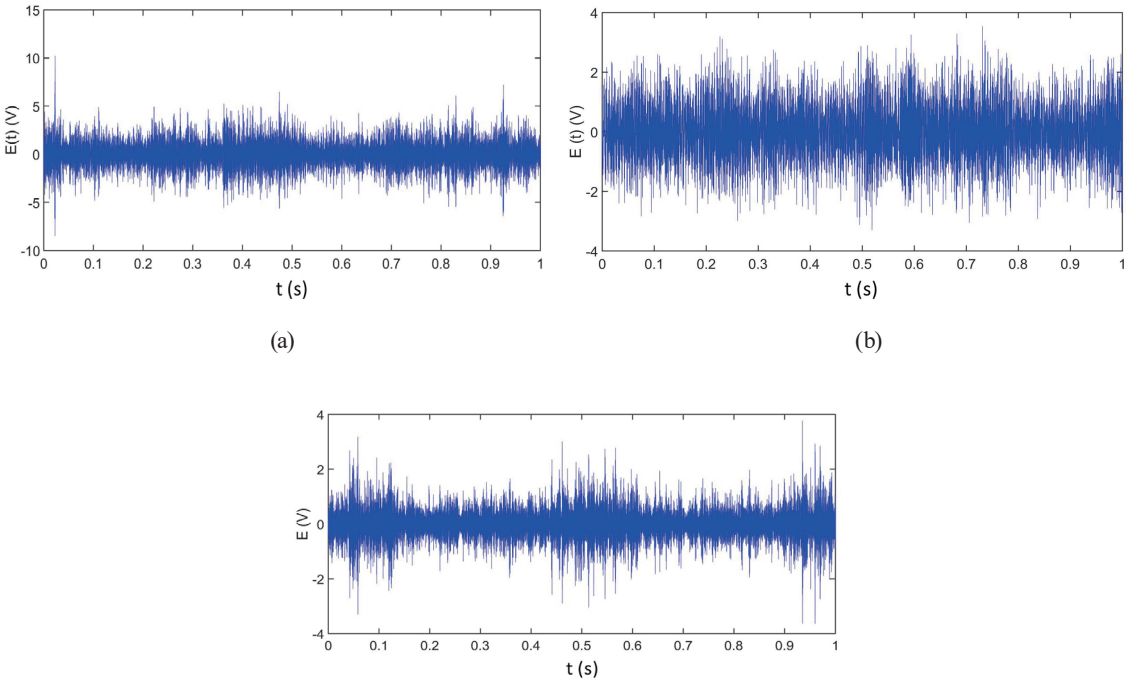


Fig. 16. (Color online) Time-domain waveforms of the measured AE signal at 50 Hz with the applied load of $L_{max}$ for different gear lubricants: (a) L-TSA32, (b) L-TSA46, and (c) L-TSA68.

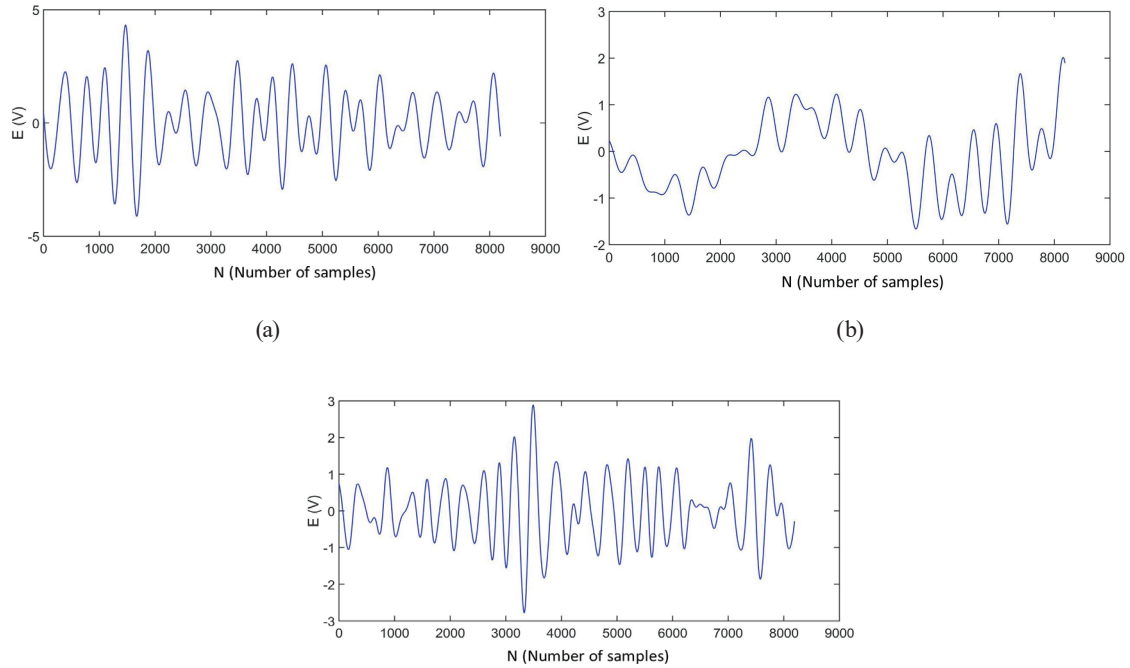


Fig. 17. (Color online) Time-domain waveforms of the reconstructed AE signal with noise reduction at 50 Hz with the applied load of $L_{max}$ for different gear lubricants: (a) L-TSA32, (b) L-TSA46, and (c) L-TSA68.

10 V. In contrast, when the viscosity of the adopted lubricant (such as the L-TSA68 turbine oil) is high, the maximum absolute electrical voltage of the AE signal does not exceed 5 V.

On the basis of the above data, we used the proposed ESED method with 8192 samples to reduce the noise of the measured AE signals. The resultant time-domain waveform of AE signals after noise reduction is shown in Fig 17. It is seen that the whole amplitudes of AE signals after noise reduction increase with decreasing lubricant viscosities. The reason is that, as the lubricant viscosity decreases, the thickness of the lubricating oil film decreases and direct contact occurs among the micro-convex parts of tooth surfaces, which cause an increase in the signal intensity as well as the electrical voltage.

## 5. Conclusion

We proposed a novel NRM based on the ESED scheme and the SVD method to effectively analyze the AE signals from operating gears so as to understand the wear conditions of gear surfaces in real time. For the AE signal measurement and analysis, we built an AE signal acquisition system including a major AE sensor and performed real-time experiments via this system. Through the manipulation of detected AE data by NRM, we have three findings. First, the signal analysis in the time-domain reveals that the energy and electrical voltage of the AE signal increase with motor speed or applied load. However, the energy and voltage of the AE signal decrease with increasing lubricant viscosity. Second, the signal analysis in the frequency domain reveals that, for all tested lubricants, the noise reduction mainly occurs at 0–10 KHz, and when the motor speed or the applied load increases, the signal frequency distribution becomes more dispersed and the maximum absolute voltage of the signal appearing at about 6 KHz gradually decreases.

## Acknowledgments

This work was supported in part by the National Natural Science Foundation of China under Grant no. 51775114, in part by the Natural Science Foundation of Fujian Province under Grant no. 2019J01822, in part by the Technology Plan Guiding Project of Sanming under Grant no. 2020-G-58, in part by the Sanming University of Fujian Province, China, under Grant no. 19YG05, and in part by the Department of Science and Technology of Fujian Province under Grant nos. 2020-H-0049, 2021-H-0060, and 2021-G-02013.

## References

1 W. Kaiser: IEEE J. Quantum Electron. **4** (1968) 381. https://doi.org/10.1109/JQE.1968.1075273
2 F. J. Guild, D. Walton, R. D. Adams, and D. Short: Composites **7** (1976) 173. https://doi.org/10.1016/0010-4361(76)90065-3
3 B. S. Ram and P. Anand: Eng. Fail. Anal. **86** (2018) 1. https://doi.org/10.1016/j.engfailanal.2017.12.016
4 A. B. Novoa and C. M. Vicuña: Insight J. **58** (2016) 18. https://doi.org/10.1784/insi.2016.58.1.18
5 R. Li, S. U. Seçkiner, D. He, E. Bechhoefer, and P. Menon: IEEE Trans. Syst. Man, Cybern. Part C Appl. Rev. **42** (2012) 1308. https://doi.org/10.1109/TSMCC.2011.2182609
6 D. Gu, J. Kim, Y. An, and B. K. Choi: J. Mech. Sci. Technol. **25** (2011) 1279. https://doi.org/10.1007/s12206-011-0231-4

7 M. D. Prieto and D. Z. Millán: IEEE Trans. Ind. Electron. **64** (2017) 8707. https://doi.org/10.1109/TIE.2017.2701761
8 D. Mba: Shock Vib. Digest. **38** (2006) 3. https://doi.org/10.1177/0583102405059054
9 D. Mba: NDT & E Int. **35** (2002) 293. https://doi.org/10.1016/S0963-8695(01)00053-6
10 F. Leaman, C. M. Vicuña, R. Baltes, and E. Clausen: J. Vib. Control **25** (2019) 2295. https://doi.org/10.1177/1077546319852536
11 C. M. Vicuña: Appl. Acoust. **77** (2014) 150. https://doi.org/10.1016/j.apacoust.2013.04.017
12 C. K. Tan, P. Irving, and D. Mba: Mech. Syst. Signal Process. **21** (2007) 208. https://doi.org/10.1016/j.ymssp.2005.09.015
13 M. S. Raghav and R. D. Sharma: Arch. Comput. Methods Eng. **28** (2020) 2845. https://doi.org/10.1007/s11831-020-09480-8
14 J. Li, X. Wang, N. Shen, H. Gao, C. Zhao, and Y. Wang: Int. J. Adv. Manuf. Technol. **98** (2018) 5. https://doi.org/10.1007/s00170-018-2383-1
15 J. A. Steel and R. L. Reuben: J. Strain Anal. Eng. Des. **40** (2005) 45. https://doi.org/10.1243/030932405X7647
16 G. Ciaburro and G. Iannace: Appl. Sci. **12** (2022) 10476. https://doi.org/10.3390/app122010476
17 N. Vahid, A. Samuel, K. Siavash, S. Farrokh, and A. Stergios: Constr. Build. Mater. **350** (2022) 128877. https://doi.org/10.1016/j.conbuildmat.2022.128877
18 V. Els, V. S. Charlotte, V. Eline, and W. Martine: Constr. Build. Mater. **349** (2022) 128732. https://doi.org/10.1016/j.conbuildmat.2022.128732
19 M. Chai, X. Hou, Z. Zhang, and Quan Duan: Int. J. Fatigue **160** (2022) 106860. https://doi.org/10.1016/j.ijfatigue.2022.106860
20 O. AlShorman, F. Alkahatni, M. Masadeh, M. Irfan, A. Glowacz, J. Kozik, and W. Glowacz: Adv. Mech. Eng. **13** (2021). https://doi.org/10.1177/1687814021996915
21 Y. Wang, J. Q. Han, Z. Y. Song, and C. Zhu: Eng. Fract. Mech. **258** (2021) 108074. https://doi.org/10.1016/j.engfracmech.2021.108074
22 H. Shao, H. Jiang, H. Zhao, and F. Wang: Mech. Syst. Signal Process. **95** (2017) 187. https://doi.org/10.1016/j.ymssp.2017.03.034
23 S. A. Shevchik, G. Masinelli, C. Kenel, C. Leinenbach, and K. Wasmer: IEEE Trans. Ind. Inf. **15** (2019) 5194. https://doi.org/10.1109/TII.2019.2910524
24 R. I. R. Hamzaha and D. Mba: Insight **50** (2008) 642. https://doi.org/10.1784/insi.2008.50.11.642
25 D. Li, Y. Wang, W. J. Yan, and W. X. Ren: Struct. Health Monit. **20** (2021) 1563. https://doi.org/10.1177/1475921720922797
26 Y. Fan, F. Gu, and A. Ball: Wear **268** (2010) 811. https://doi.org/10.1016/j.wear.2009.12.010
27 Z. He, K. Zhao, Y. Yan, F. Ning, Y. Zhou, and Y. Song: Constr. Build. Mater. **288** (2021) 123119. https://doi.org/10.1016/j.conbuildmat.2021.123119
28 F. König, C. Sous, A. Ouald Chaib, and G. Jacobs: Tribol. Int. **155** (2021) 106811. https://doi.org/10.1016/j.triboint.2020.106811
29 Y. Xiao, B. Wu, J. Shi, L. Wang, and H. L. Liu: Int. J. Geomech. **23** (2023) 0423153-1. https://doi.org/10.1061/IJGNAI.GMENG-8817
30 S. Sikdar, D. Liu, and A. Kundu: Composites, Part B **228** (2022) 109450. https://doi.org/10.1016/j.compositesb.2021.109450
31 Z. Liu, X. Wang, and L. Zhang: IEEE Trans. Ind. Inf. **69** (2020) 6630. https://doi.org/10.1109/TIM.2020.2969062
32 H. Li, Y. Qiao, R. Shen, M. He, T. Cheng, Y. Xiao, and J. Tang: Geology **294** (2021) 106386. https://doi.org/10.1016/j.enggeo.2021.106386
33 Z. Ge and Q. Sun: Int. J. Rock Mech. Min. Sci. **138** (2021) 1365. https://doi.org/10.1016/j.ijrmms.2021.104616
34 Z. H. Zhang and J. H. Deng: Int. J. Rock Mech. Min. Sci. **130** (2020) 1365. https://doi.org/10.1016/j.ijrmms.2020.104323
35 K. Du, X. Li, M. Tao, and S. Wang: Int. J. Rock Mech. Min. Sci. **133** (2020) 1365. https://doi.org/10.1016/j.ijrmms.2020.104411